JACS
JOURNAL OF THE AMERICAN CHEMICAL SOCIETY

Article

pubs.acs.org/JACS

Selective Visualization of the Endogenous Peroxynitrite in an Inflamed Mouse Model by a Mitochondria-Targetable Two-Photon Ratiometric Fluorescent Probe

Dan Cheng,[†] Yue Pan,[†] Lu Wang,[‡] Zebing Zeng,[†] Lin Yuan,*[,†] Xiaobing Zhang,[†] and Young-Tae Chang[‡,§]

[†]State Key Laboratory of Chemo/Biosensing and Chemometrics, College of Chemistry and Chemical Engineering, Hunan University, Changsha 410082, P. R. China

[‡]Department of Chemistry and Medicinal Chemistry Programme, National University of Singapore, Singapore 117543, Singapore

[§]Laboratory of Bioimaging Probe Development, Singapore Bioimaging Consortium, Singapore 117543, Singapore

Supporting Information

ABSTRACT: Peroxynitrite ($ONOO^-$) is a kind of reactive oxygen species (ROS) with super activity of oxidization and nitration, and overproduction of $ONOO^-$ is associated with pathogenesis of many diseases. Thus, accurate detection of $ONOO^-$ with high sensitivity and selectivity is imperative for elucidating its functions in health or disease states. Herein we for the first time present a new two-photon ratiometric fluorescent $ONOO^-$ probe (**MITO-CC**) based on FRET mechanism by combining rational design strategy and dye-screening approach. **MITO-CC**, with fast response rate (within 20 s), excellent sensitivity (detection limit = 11.30 nM) and outstanding selectivity toward $ONOO^-$, was successfully applied to ratiometric detection of endogenous $ONOO^-$ produced by HepG2/RAW264.7 cells and further employed for imaging oxidative stress in an inflamed mouse model. Therefore, probe **MITO-CC** could be a potential biological tool to explore the roles of $ONOO^-$ under different physiological and pathological settings.

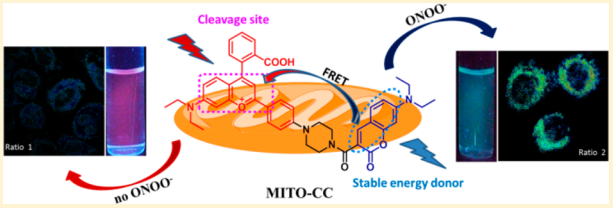

INTRODUCTION

Peroxynitrite ($ONOO^-$), a kind of reactive oxygen species (ROS) with strong oxidizability and nucleophilicity, is formed by the combination of both nitric oxide (NO) and superoxide anion radical ($O_2^{\bullet-}$) under diffusion control without enzymatic catalysis.[1] It is balanced with its protonated form ONOOH (pK_a 6.8),[2] and has a short half-life (about 1 s) at pH 7.4,[3,4] whereas it can react with many bioactive species, such as proteins, nucleic acids, lipids, etc. This is because of not only the oxidation and nucleophilic properties of $ONOO^-$, and also its translation ability into highly active secondary radicals, including hydroxyl radical ($^{\bullet}OH$), nitrogen dioxide ($^{\bullet}NO_2$) and carbonate radicals ($CO_3^{\bullet-}$), which will further interact with biomolecules, eventually resulting in cellular apoptosis. Accordingly, $ONOO^-$ has been implicated in detection of various clinical diseases, such as inflammatory, Alzheimer's disease, cancer, and autoimmune.[5−7] An increasing number of studies have revealed that $ONOO^-$ also plays an active role in signal transduction via nitrating tyrosine residues and immunogenic response against pathogen invasion.[8−11] Nevertheless, the dualistic role of $ONOO^-$ is still controversial and the biological activities of $ONOO^-$ have not yet been fully revealed.[12] Thus, development of effective methods for detecting $ONOO^-$ is very conducive to explore the physiological mechanism of in vivo $ONOO^-$ and investigate its role in related diseases.[7]

Recently, fluorescent probes have attracted a great deal of attention due to the superiorities of simple operation, high sensitivity, real-time and nondestructive detection.[13−17] With the development of molecular fluorescence technology, a number of small-molecule fluorescent probes for $ONOO^-$ have been reported. These probes are mainly based on a protected/deprotected strategy to detect $ONOO^-$, such as the trifluorocarbonyl-based, the boronic acid ester-based and *N*-phenylrhodol-based probes.[18−25] They are initially nonfluorescent stemming from the protected fluorophores, while reacting with $ONOO^-$ will turn on their fluorescence through releasing the uncaged-fluorophore, which is used to detect $ONOO^-$ by measuring the changes of fluorescence signal. Some fluorophores, such as cyanine[26−28] or hemicyanine,[29] can be also used directly as responding groups due to the rapid destruction of these fluorophores in the presence of $ONOO^-$. Meanwhile, $ONOO^-$ probes based on other methods also exist.[30−38] However, owing to the similar properties from other ROS including HOCl and H_2O_2, distinguishing detection of $ONOO^-$ remains a big challenge, especially in multiple ROS coexisted physiological environment.[39−42] Therefore, it has been of focus and difficulty to develop fluorescent probes with high sensitivity and excellent selectivity for tracing $ONOO^-$

Received: October 12, 2016
Published: December 5, 2016

DOI: 10.1021/jacs.6b10508
J. Am. Chem. Soc. 2017, 139, 285−292

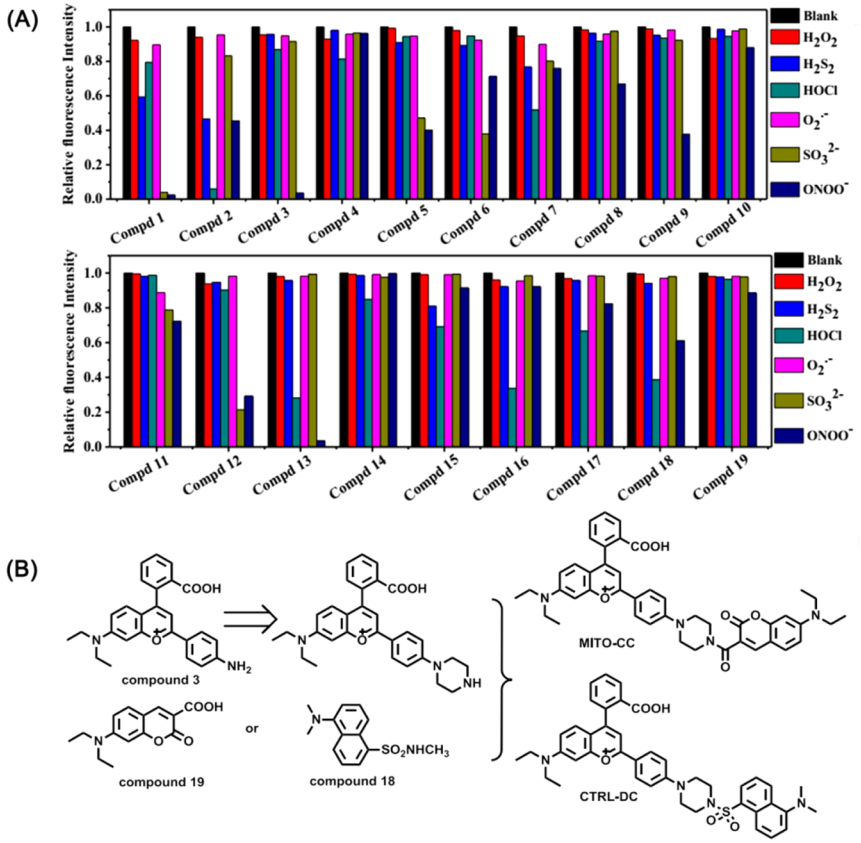

Figure 1. (A) Relative fluorescence intensities of compounds **1**−**19** (5 μM) for various agents in aqueous solution buffered at physiological pH (25 mM phosphate buffer, mixed with 30% ethanol, pH 7.4). H_2O_2, 100 μM; H_2S_2, 50 μM; HOCl, 100 μM; $O_2^{\bullet-}$, 100 μM; SO_3^{2-}, 150 μM; ONOO$^-$, 25 μM. (B) Design and structures of compounds **MITO-CC** and **CTRL-DC**.

level in biological samples. Comparing with the conventional intensity-based probes, fluorescence resonance energy transfer (FRET) is one of the most popular fluorescent mechanism for designing ratiometric probes.[43] This strategy can eliminate the adverse effects induced by probe concentration, probe environment and excitation intensity through a built-in calibration of two emission bands, thereby providing an ideal method to quantitively detect biomolecules.[44−46] In addition, two-photon excitation (TPE) probe can facilitate three-dimensional (3D) fluorescence imaging of living biological sample, endowed with weak photodamage to biosamples, deep tissue penetration, and low background fluorescence.[47,48] However, to the best of our knowledge, no FRET-based fluorescent ONOO$^-$ probes with two-photon excitation have been reported yet. Therefore, it is indeed urgent to develop fluorescent FRET probes with TP absorption for in vivo ratiometric imaging of ONOO$^-$.

Herein, by combining the strategies of rational design and dye-screening, we reported a two-photon ratiometric fluorescent probe (**MITO-CC**) for ONOO$^-$ detection based on FRET system. The probe showed ultrafast response (within 20 s) toward ONOO$^-$ with high sensitivity (limit detection is 11.30 nM), and prominent selectivity to coexisted ROS (e.g., HOCl, H_2O_2, $^{\bullet}$OH) and RSS (e.g., H_2S, H_2S_2, SO_2). Furthermore, the probe was successfully applied for ratiometric imaging of mitochondrial ONOO$^-$ in living cells and visualized the small fluctuation of ONOO$^-$ level in an inflamed pathological environment by two-photon fluorescence confocal microscopy for the first time.

RESULTS AND DISCUSSION

Design and Synthesis of Probes. Many dyes, such as cyanine or hemicyanine, can be cleaved by ONOO$^-$ due to its strong oxidation and nucleophilic property, leading to design of fluorescent ONOO$^-$ probes.[49−51] However, cyanine or hemicyanine also have been demonstrated to be very susceptible to other biological species, such as ROS (e.g., HOCl)[52] and reactive sulfur species (RSS) (e.g., H_2S, SO_3^{2-}).[53−55] Thus, it is still difficult to obtain fluorescent probes with selective differentiation of ONOO$^-$ from other coexisted ROS/RSS in complex physiological environment. To solve this problem, the dye-screening approach was used to examine the response of probes to ONOO$^-$. A long wavelength fluorescent dye, with specific and sensitive response to ONOO$^-$ and a stable short wavelength dye to ROS/RSS were chosen and integrated to develop a ratiometric fluorescent probe for ONOO$^-$ through rational designing.

Nineteen self-synthesized or purchased dyes (compounds **1**−**19**, Scheme S1) were collected as the candidates for screening. Their reactivities toward representative oxidants and nucleophiles, including hydrogen peroxide (H_2O_2), hypochlorite (HOCl), superoxide anion radical ($O_2^{\bullet-}$), hydrogen persulfide (H_2S_2), sulfiteion (SO_3^{2-}) and ONOO$^-$, were evaluated by emission spectral analysis in an aqueous solution buffered at physiological pH (25 mM phosphate buffer, mixed with 30% ethanol, pH 7.4). As shown in Figure 1A and Figures S1−20, the fluorescence intensity of compound **3** decreases rapidly upon treatment with ONOO$^-$ but is almost invariant in the presence of other oxidizing and nucleophilic reagents,

DOI: 10.1021/jacs.6b10508
J. Am. Chem. Soc. 2017, 139, 285−292

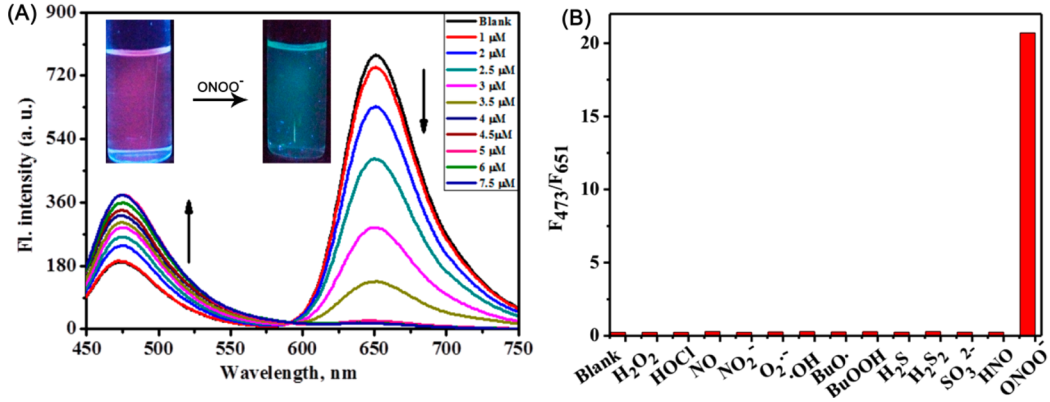

Figure 2. (A) Fluorescence spectra of **MITO-CC** (5 μM) upon addition of $ONOO^-$ (0−1.5 equiv) in pH 7.4 PBS/EtOH (v/v, 7/3). (B) Fluorescence ratio (F_{473}/F_{651}) of **MITO-CC** (5 μM) in PBS/EtOH (v/v, 7/3) toward various analytes: $ONOO^-$ (5 μM); other analytes (100 μM). The mixture were kept for 30 min at room temperature before the fluorescence intensity of the probe solution was measured. Excitation at 420 nm.

indicating the high sensitivity and selectivity of compound **3** to $ONOO^-$. Meanwhile, even compounds **8**−**10** and **14** also exhibited good selectivity to $ONOO^-$, the poor sensitivity limits their further application in biological systems. Thus, compound **3** was chosen as the energy acceptor of the FRET dyad due to its excellent responsibility to $ONOO^-$. Also, among compounds **15**−**19** with shorter wavelength (Figure 1A and Figures S16−20), we chose the easily modified coumarin (compound **19**) as the energy donor due to its stability to various species and excellent optical properties, including high molar absorbance, high fluorescence quantum yield, good photostability and solubility.[56−58] Meanwhile, dansyl fluorophore (compound **18**) was chosen to construct a negative control compound. Thus, we rationally designed and synthesized a ratiometric fluorescent $ONOO^-$ probe (**MITO-CC**) and a negative control compound (**CTRL-DC**) (Figure 1B) through fluorescence analysis and chemical synthesis (for synthetic and characterization details, see the Supporting Information).

Spectral Response of the Probes to $ONOO^-$. With probe **MITO-CC** and negative control compound **CTRL-DC** in hand, we first investigated their spectral response to $ONOO^-$. All spectrometry measurements were carried out in an aqueous solution buffered at physiological pH (25 mM phosphate buffer, mixed with 30% ethanol, pH 7.4) (Figure 2). In spectrofluorometric titrations, **MITO-CC** exhibited a strong emission band centered at 651 nm and a weak characteristic emission band of coumarin centered at 473 nm in the absence of $ONOO^-$, and the solution of probe **MITO-CC** showed a red fluorescence (Φ = 0.04). Upon addition of increasing dosages of $ONOO^-$ (0 to 7.5 μM), the emission band centered at 651 nm almost disappeared accompanied by the significant enhancement of coumarin emission (Φ = 0.08), and the fluorescence color of the solution changed from red to bluish green (Figure 2A, inset). Notably, a 93-fold fluorescence ratio (I_{473}/I_{651}) enhancement was observed with a good linear relationship over an $ONOO^-$ concentration range from 0 to 7.5 μM. The detection limitation was calculated to be 1.13×10^{-8} M (Figure S21), which indicated the high sensitivity of **MITO-CC** toward $ONOO^-$ and the capability of **MITO-CC** to detect trace amounts of intracellular $ONOO^-$. In addition, the spectral response of **CTRL-DC** to $ONOO^-$ was also investigated. As shown in Figure S22, like probe **MITO-CC**, free **CTRL-DC** showed a bright red fluorescence with a strong emission peak at 635 nm. However, when 1 equiv. $ONOO^-$ was added into the **CTRL-DC** solution (5 μM), the emission band dropped distinctly and simultaneously a weak rise at 490 nm occurred, probably because the dansyl chromophore is unstable to $ONOO^-$ (Figure 1A), indicating that a chemical stability energy donor is vital for FRET-based ratiometric detection of $ONOO^-$. Interestingly, according to reaction-time study, the change of the fluorescence intensity was completed and the intensity reached a plateau within 20 s after 1.5 equiv. $ONOO^-$ addition (Figure S23), which indicated that the probe **MITO-CC** is well suitable for $ONOO^-$ detection with high sensitivity.

To test the selectivity of **MITO-CC** for $ONOO^-$, the specificity of **MITO-CC** was evaluated in the presence of various biologically relevant ROS and RNS, including NO, $O_2^{\bullet-}$, NO_2^-, $^{\bullet}OH$, $BuO^{\bullet}$, BuOOH, H_2S, H_2S_2, SO_3^{2-}, HNO, H_2O_2 and HOCl. As shown in Figure 2B, **MITO-CC** exhibited negligible fluctuation of fluorescence ratio (F_{473}/F_{651}) even upon treatment with 100 μM of these interfering species. However, a remarkable enhancement was observed after treated with only 5 μM $ONOO^-$, which suggested probe **MITO-CC** has superior selectivity for $ONOO^-$. Notably, fluorescence titration experiments showed that the probe can avoid the interference from H_2O_2 with a broad concentration range from 0 to 500 μM (Figure S24). H_2O_2 has been the main interfering substance in terms of peroxynitrite detection. The superior selectivity should be attributed to the stronger nucleophilicity of $ONOO^-$ than H_2O_2, and thus $ONOO^-$ react more easily with unsaturated compounds. Moreover, the fluorescence titration experiments of probe **MITO-CC** toward $ONOO^-$ was also investigated in phosphate buffer containing 1% DMSO at physiological pH, which simulated physiological condition. As shown in Figure S25, the similar spectral change was also observed after treated with increasing dosages of $ONOO^-$. In addition, to mimic the viscosity of biological system especially in mitochondria, the fluorescence response of probe **MITO-CC** toward $ONOO^-$ has also been examined in a PBS/glycerol (4/6, v/v) mixed solvent (pH 7.4).[59,60] The spectrofluorometric titrations, including excitation and emission spectra, demonstrated that **MITO-CC** shows a good optical response toward $ONOO^-$ in mitochondrial viscous environment (Figures S26 and S27A). **MITO-CC** also displays superior selectivity for $ONOO^-$ over other ROS and RNS in this environment (Figure S27B). These results implied that **MITO-CC** is feasible for detection of $ONOO^-$ in biological system. In addition, the pH effect on the response of **MITO-CC** to $ONOO^-$ was tested. Upon addition of $ONOO^-$ to **MITO-CC** solution, compatible

DOI: 10.1021/jacs.6b10508
J. Am. Chem. Soc. 2017, 139, 285−292

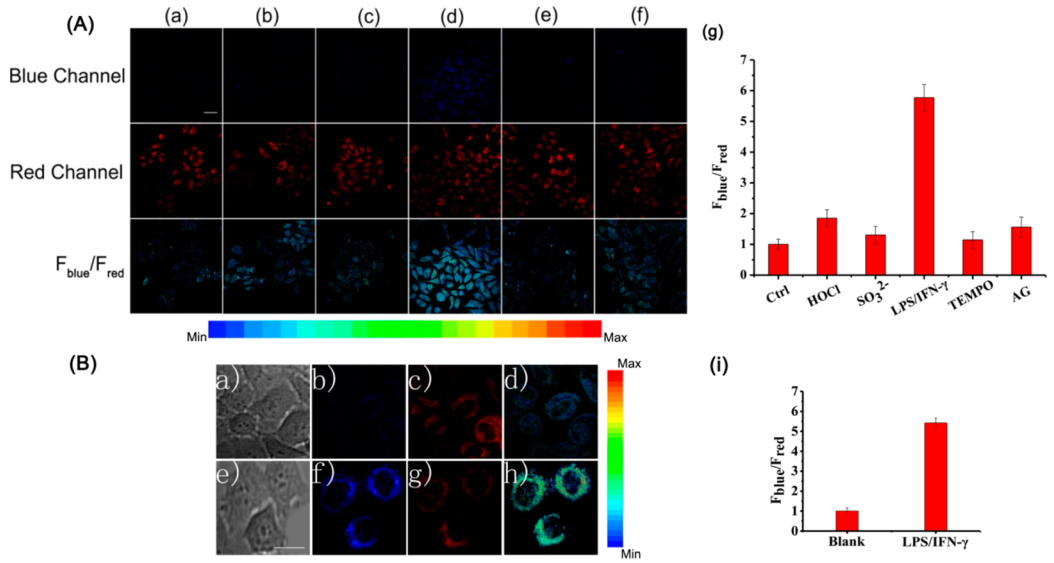

Figure 3. (A) Fluorescence images of probe **MITO-CC** in HepG2 cells under different conditions by confocal fluorescence images. (a) Cells were incubated with probe **MITO-CC** (5 μM, 20 min), then imaged. (b, c) Cells were pretreated with probe **MITO-CC** (5 μM, 20 min), subsequently incubated with NaOCl (100 μM) (b) and SO_3^{2-} (100 μM) (c) for 20 min, then imaged. (d) Cells were prestimulated with LPS (1 μg/mL) and IFN-γ (50 ng/mL) for 12 h, subsequently incubated with probe **MITO-CC** (5 μM, 20 min), then imaged. (e, f) Cells pretreated with $O_2^{\bullet-}$ scavenger TEMPO (300 μM) (e) or NOS inhibitor AG (5 mM) (f) during stimulation with LPS (1 μg/mL)/IFN-γ (50 ng/mL) for 12 h, subsequently incubated with probe **MITO-CC** (5 μM, 20 min), then imaged. The fluorescence images were captured from the blue channel of 445−490 nm and red channel of 630−675 nm with an excitation at 405 nm. Third row: F_{blue}/F_{red} ratiometric images. (g) Average fluorescence intensity ratios (F_{blue}/F_{red}) of in panel A(a−f). Data are mean ± S.E.M., n = 3. (B) Two-photon confocal fluorescence images of $ONOO^-$ in HepG2 cells incubated with only **MITO-CC** (5.0 μM) (a−c) or coincubated with LPS (1 μg/mL) and IFN-γ (50 ng/mL) (e−g) with an excitation at 800 nm. First column, bright-field images. Second column, the fluorescence images of blue channel collected at 460−500 nm. Third column, the fluorescence images of red channel collected at 605−680 nm. Forth column, the ratiometric images (F_{blue}/F_{red}). (i) Average F_{blue}/F_{red} intensity ratios in panel B(d, h). Data are expressed as mean ± SD of three experiments. Scale bar: 20 and 10 μm panels A and B, respectively.

enhancement of fluorescence ratio (F_{478}/F_{654}) was observed at pH 6−9 (Figure S28), which indicated the probe can monitor $ONOO^-$ in physiological pH.

Proposed Mechanism. According to the literature,[19] $ONOO^-$ might trigger subsequent nucleophilic addition, oxidation, elimination, and hydrolysis reactions on chromenylium fluorophore due to its nucleophilicity and oxidizability, and finally yields an olefine acid product (Scheme S3 and S4). To confirm our assumption, the reaction mixture of compound **3** and $ONOO^-$ was first analyzed by mass spectrometry. As expected, the peak of our proposed product, olefine acid (m/z = 378.7, $[M + Na]^+$) was observed (Figure S29). Moreover, the mixture of **MITO-CC** and $ONOO^-$ was also analyzed by mass spectrometry, and the peaks of two key products, olefine acid (m/z = 378.7, $[M + Na]^+$) and coumarin (m/z = 422.6, $[M + H]^+$) were also observed (Figure S30). Thus, the results are in good agreement with the proposed mechanism (Schemes S3 and S4).

Fluorescence Imaging of Endogenous $ONOO^-$ Production in HepG2 and RAW264.7 Cells. Due to the special property of $ONOO^-$, the steady-state concentrations of $ONOO^-$ are estimated to be in the nanomolar concentration range in physiological condition.[61] And the rates of peroxynitrite production in vivo in specific compartments have been estimated to be as high as 50−100 μM per min.[62] Encouraged by the above promising results in vitro (e.g., fast response rate (within 20 s), excellent sensitivity (detection limit = 11.30 nM) and high selectivity), we then investigated the capability of **MITO-CC** for detecting endogenously produced $ONOO^-$ in a dual-color manner by confocal fluorescence microscopy. Before that, the cell cytotoxity of **MITO-CC** was evaluated by standard MTT assays, which demonstrated that **MITO-CC** possesses low cytotoxicity to living HepG2 cells (Figure S31). To eliminate latent interference induced by other biological relevant ROS and RSS, the selectivity of **MITO-CC** to visualize $ONOO^-$ was validated in living HepG2 cells. HOCl and SO_3^{2-} were selected as the representative interfering ROS and RSS in this study, and the production of endogenous $ONOO^-$ was stimulated by bacterial endotoxin lipopolysaccharide (LPS) and pro-inflammatory cytokine interferon-gamma (IFN-γ).[63] As shown in Figure 3A, HepG2 cells incubated with only probe **MITO-CC** showed negligible fluorescence in blue channel but strong fluorescence in red channel. However, a dramatic fluorescence enhancement of blue channel and slightly decreased fluorescence of red channel were observed when the cells were prestimulated with LPS/IFN-γ before incubation with probe **MITO-CC**. The signal ratio (F_{blue}/F_{red}) was also calculated, showing a 5.8-fold enhancement (Figure 3A(g)). In contrast, the cells exhibited minor fluorescence changes in the both channels when pretreated with HOCl or SO_3^{2-} before incubation with probe **MITO-CC**. It is evident that the increased signal ratio (F_{blue}/F_{red}) is mainly due to the reaction between probe and stimulation-generated $ONOO^-$, demonstrating the feasibility of **MITO-CC** to specially monitor $ONOO^-$ in living systems. To validate further the above assumption, control experiments were performed, in which 2,2,6,6-tetramethylpiperidine-*N*-oxyl (TEMPO), a superoxide ($O_2^{\bullet-}$) scavenger,[64] and aminoguanidine (AG), a nitric oxide synthase (NOS) inhibitor,[64] were added to decrease cellular $ONOO^-$. As shown in Figure 3A(e, f), the cellular fluorescence intensities of **MITO-CC** stained cells remain unchanged in both blue and red channels

DOI: 10.1021/jacs.6b10508
J. Am. Chem. Soc. 2017, 139, 285−292

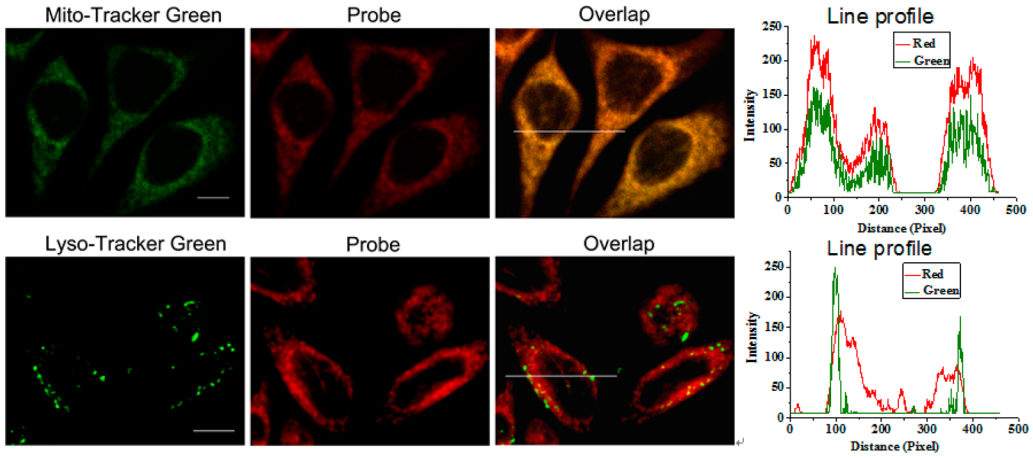

Figure 4. Intracellular localization of **MITO-CC** in HepG2 cells. Images of HepG2 cells pretreated respectively with 5 μM **MITO-CC** for 20 min and subsequently 1 μM Mito-Tracker Green (or 1 μM Lyso-Tracker Green) for 10 min. Green channel, Mito-Tracker Green and Lyso-Tracker Green fluorescence (λ_{ex}= 488 nm, λ_{em} = 500−535 nm); red channel, probe fluorescence (λ_{ex} = 405 nm, λ_{em} = 630−675 nm); yellow, merged signal. Line profile: intensity profile of the white line in image overlap. Scale bar: 10 μm.

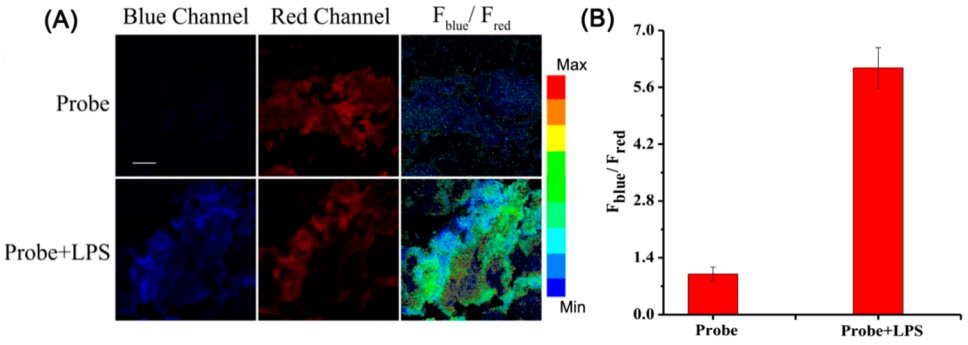

Figure 5. (A) Two-photon fluorescence images of a fresh rat liver slice with a magnification of 10×. One group tissues were treated only **MITO-CC** (10 μM) for 30 min and another group pretreated with 200 μL LPS for 12 h and then with probe **MITO-CC** (10 μM) incubated for 30 min. (B) Average ratio values of fluorescence intensity (F_{blue}/F_{red}) in panel A. Excitation at 800 nm. Emission band at 460−500 nm in the blue channel and 605−680 nm in the red channel. Scale bar: 200 μm.

when the stimulated cells were incubated with TEMPO or AG. This is mainly because of the inhibition effect of TEMPO and AG on the cellular $ONOO^-$ production. To investigate further the above assumption, control experiment of inhibiting cellular HOCl formation was performed. As shown in Figure S32, almost no change of intracellular fluorescence ratio was observed when the stimulated cells were coincubated with 4-aminobenzoicacid (ABH), an myeloperoxidase inhibitor.[65] In short, these results implied that **MITO-CC** is well-suited for specifically imaging endogenous $ONOO^-$ in living cells.

Next, the feasibility of **MITO-CC** for detecting endogenous $ONOO^-$ was examined by two-photon confocal fluorescence microscopy. To verify the most appropriate two-photon excitation wavelength, the fluorescence changes of **MITO-CC** and coumarin donor (compound **19**) were evaluated in the excitation range of 760−940 nm, respectively. As shown in Figure S33, the relatively strong fluorescence was observed in both **MITO-CC** and compound **19** excited at 800−825 nm, suggesting probe **MITO-CC** is feasible for two-photon fluorescence imaging. The HepG2 cells incubated with probe **MITO-CC** (5 μM) displayed weak fluorescence in the blue channel (Figure 3B(b)) and strong fluorescence in the red channel (Figure 3B(c)) upon excitation at 800 nm. However, the HepG2 cells prestimulated with LPS/IFN-γ, showed an increased fluorescence of blue channel and a relatively attenuated fluorescence of red channel (Figure 3B(f,g)) accompanied by a dramatic enhancement of signal ratio (F_{blue}/F_{red}) (Figure 3B(d,h)). This phenomenon was consistent with the fluorescence imaging of endogenous $ONOO^-$ by one-photon confocal fluorescence microscopy (Figure S34). We also confirmed that **MITO-CC** could be employed to image LPS/IFN-γ endogenous $ONOO^-$ in RAW264.7 cells (Figure S35). Thus, **MITO-CC** is capable of detecting $ONOO^-$ by two-photon imaging in living cells.

Having performed the $ONOO^-$ imaging in cells, we proceeded to confirm the distribution of $ONOO^-$ at subcellular levels, by conducting colocalization experiments in HepG2 cells. The cells were pretreated with 5 μM **MITO-CC** for 20 min and subsequently 1 μM Mito-Tracker Green (or 1 μM Lyso-Tracker Green) for 10 min. As expected, the fluorescence of **MITO-CC** in red channel overlapped exactly with that of Mito-Tracker Green in green channel (overlap coefficient 0.80) but not with that of lysosome (Figure 4), resulting from the charge attraction between **MITO-CC** with a positive charge and cellular mitochondrial membrane with the negative potential.[66] Meanwhile, the same subcellular distribution of **MITO-CC** can also be confirmed in HeLa cells (Figure S36). Recently, mitochondria is considered as the dominant organelle for $ONOO^-$ formation and reactions in living cell;[67] thus, this

DOI: 10.1021/jacs.6b10508
J. Am. Chem. Soc. 2017, 139, 285−292

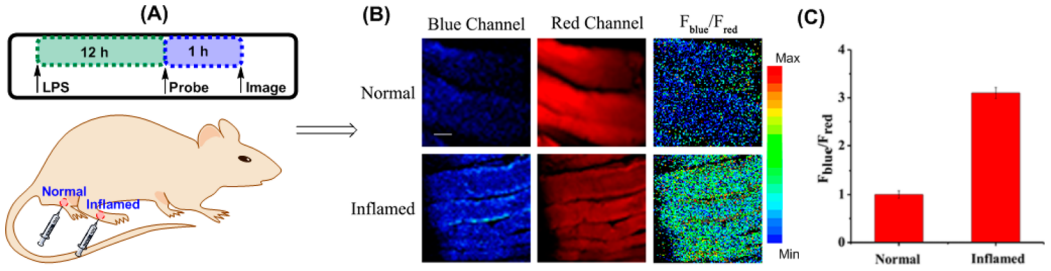

Figure 6. Two-photon confocal microscopic fluorescence images for detecting of LPS-dependent $ONOO^-$ generation in inflammation tissues via **MITO-CC**. (A) 200 μL of LPS (1 mg/mL) was subcutaneously injected into right leg of mice to cause inflammation. After 12 h, 20 μL of 500 μM **MITO-CC** was subcutaneously injected in situ. After 1 h, the leg skin of mice was sectioned after being anaesthetized. (B) Fluorescence images of **MITO-CC** in the normal and inflamed tissues. (C) Average F_{blue}/F_{red} intensity ratios in panel B. Blue channel, λ_{em} = 460−500 nm; red channel, λ_{em} = 605−680 nm. λ_{ex} = 800 nm. Scale bar: 200 μm.

probe offers an excellent tool for detecting mitochondrial $ONOO^-$.

Two-Photon Living Hepatic Tissue Imaging of Endogenous $ONOO^-$. Besides the living cell study, the ability of **MITO-CC** to detect $ONOO^-$ in living tissues was examined as well. To this end, the living liver tissues were prepared for one-photon and two-photon fluorescence microscopy (TPFM) analysis. The experiments were divided into two groups. In the first control group, the liver tissues were incubated with only probe **MITO-CC** (10 μM) for 30 min in PBS, and the results of two-photon fluorescence imaging showed a weak fluorescence in the blue channel and bright fluorescence in the red channel (Figures 5A and S37A). In the second group, after the liver tissues were pretreated with LPS (200 μL, 1 mg/mL) for 12 h and then coincubated with **MITO-CC** (10 μM) for 30 min, a distinct fluorescence increase in the blue channel and a slight fluorescence decrease in red channel were observed, respectively (Figures 5A and S37B), and the enhancement of ratiometric signals (F_{blue}/F_{red}) was up to 6.10-fold (Figure 5B). Moreover, the changes of the fluorescence signals could be detected in liver tissues within a depth of 110 μm (Figure S37). On the contrary, in the one-photon mode, the changes of the fluorescence signals are detected only in 70 μm depth (Figure S38). These results demonstrated that **MITO-CC** is capable of rendering the visualization of $ONOO^-$ in living liver tissues at the depth of 110 μm using TPFM, further extending its applicability in fluorescence bioimaging studies.

Two-Photon Imaging of $ONOO^-$ in Inflamed Living Mouse Model. Finally, we applied **MITO-CC** to image $ONOO^-$ in living mouse. In an inflammatory pathological process, $ONOO^-$ may form and influence profoundly inflammatory responses at many levels.[61] However, there still few direct evidence to justify $ONOO^-$ formation under inflammation conditions. To straighten out this matter, the inflamed mouse model was used to study the connection between inflammation and $ONOO^-$ formation. The right leg of a Kunming mouse was subcutaneously injected with 200 μL LPS (1 mg/mL) to induce inflammation.[65] After 12 h, **MITO-CC** (20 μL, 500 μM) was injected via subcutaneous injection for 1 h, then the mice were anesthetized, the leg skin was sectioned for the latter two-photon fluorescence imaging. As shown in Figure 6, an obviously enhanced fluorescence of blue channel (λ_{em} = 460−500 nm) and a relatively weak fluorescence signal of red channel (λ_{em} = 605−680 nm) were observed, upon excitation at 800 nm in the inflamed tissue. Additionally, the legs of anesthesia mice were imaged directly after **MITO-CC** (20 μL, 500 μM) was injected 1 h later by TPFM, showing different fluorescence changes between control and experiment groups (Figure S39).

CONCLUSION

In summary, by combining the strategies of reasonable design and dye-screening, we have developed a two-photon ratiometric fluorescent probe, **MITO-CC**, for selectively detecting $ONOO^-$ in test tube and biological contexts. The ratiometric probe based on FRET mechanism exhibits not only outstanding sensitivity (11.30 nM), fast response (within 20 s) toward $ONOO^-$ but also high selectivity upon other various biological ROS and RNS in a physiological pH aqueous solution. The perfect performance in both cells and tissues imaging illustrated that probe **MITO-CC** can be applied to monitor endogenous $ONOO^-$ with minimal cytotoxicity either by one-photon or two-photon fluorescence confocal microscopy. Moreover, probe **MITO-CC** is capable of monitoring $ONOO^-$ produced by LPS stimulation in the inflamed mouse model. This probe is highly promising to be useful for biological imaging for disclosing the roles of $ONOO^-$ in various physiological and pathological conditions.

ASSOCIATED CONTENT

Supporting Information

The Supporting Information is available free of charge on the ACS Publications website at DOI: 10.1021/jacs.6b10508.

Experimental details for chemical synthesis of all compounds, supplementary photophysical characterization of all probes, and imaging methods and data (PDF)

AUTHOR INFORMATION

Corresponding Author

*lyuan@hnu.edu.cn

ORCID

Zebing Zeng: 0000-0002-9788-1988

Lin Yuan: 0000-0002-1015-5319

Author Contributions

The paper was written through contributions of all authors. All authors have given approval to the final version of the paper.

Notes

The authors declare no competing financial interest.

ACKNOWLEDGMENTS

This work was financially supported by NSFC (21622504, 21302050), the Hunan Provincial Natural Science Foundation of China (14JJ2047), the Hunan University Fund for

DOI: 10.1021/jacs.6b10508
J. Am. Chem. Soc. 2017, 139, 285−292

Multidisciplinary Developing (2015JCA04), and the Fundamental Research Funds for the Central Universities.

REFERENCES

(1) Radi, R. *J. Biol. Chem.* **2013**, *288*, 26464−26472.
(2) Radi, R.; Beckman, J. S.; Bush, K. M.; Freeman, B. A. *J. Biol. Chem.* **1991**, *266*, 4244−4250.
(3) Ducrocq, C.; Blanchard, B.; Pignatelli, B.; Ohshima, H. *Cell. Mol. Life Sci.* **1999**, *55*, 1068−1077.
(4) Masumoto, H.; Kissner, R.; Koppenol, W. H.; Sies, H. *FEBS Lett.* **1996**, *398*, 179−182.
(5) Pacher, P.; Beckman, J. S.; Liaudet, L. *Physiol. Rev.* **2007**, *87*, 315−424.
(6) Nagano, T. *J. Clin. Biochem. Nutr.* **2009**, *45*, 111−124.
(7) Ferrer-Sueta, G.; Radi, R. *ACS Chem. Biol.* **2009**, *4*, 161−177.
(8) Alvarez, M. N.; Peluffo, G.; Piacenza, L.; Radi, R. *J. Biol. Chem.* **2011**, *286*, 6627−6640.
(9) Fang, F. C. *Nat. Rev. Microbiol.* **2004**, *2*, 820−832.
(10) Liaudet, L.; Vassalli, G.; Pacher, P. *Front. Biosci.* **2008**, *14*, 590−605.
(11) Allen, R. G.; Lafuse, W. P.; Powell, N. D.; Webster Marketon, J. I.; Stiner-Jones, L. T. M.; Sheridan, J. F.; Bailey, M. T. *Infect. Immun.* **2012**, *80*, 3429−3437.
(12) Darrah, P. A.; Hondalus, M. K.; Chen, Q. P.; Ischiropoulos, H.; Mosser, D. M. *Infect. Immun.* **2000**, *68*, 3587−3593.
(13) Yang, Y. M.; Zhao, Q.; Feng, W.; Li, F. Y. *Chem. Rev.* **2013**, *113*, 192−270.
(14) Demchenko, A. P. *Introduction to fluorescence sensing*; Springer, 2015.
(15) Ueno, T.; Nagano, T. *Nat. Methods* **2011**, *8*, 642−645.
(16) Zhu, H.; Fan, J. L.; Du, J. J.; Peng, X. J. *Acc. Chem. Res.* **2016**, *49*, 2115−2126.
(17) Wan, Q. Q.; Chen, S. M.; Shi, W.; Li, L. H.; Ma, H. M. *Angew. Chem., Int. Ed.* **2014**, *53*, 10916−10920.
(18) Yang, D.; Tang, Y. C.; Chen, J.; Wang, X. C.; Bartberger, M. D.; Houk, K. N.; Olson, L. *J. Am. Chem. Soc.* **1999**, *121*, 11976−11983.
(19) (a) Yang, D.; Wang, H. L.; Sun, Z. N.; Chung, N. W.; Shen, J. G. *J. Am. Chem. Soc.* **2006**, *128*, 6004−6005. (b) Dong, B. L.; Song, X. Z.; Kong, X. Q.; Wang, C.; Tang, Y. H.; Liu, Y.; Lin, W. Y. *Adv. Mater.* **2016**, *28*, 8755−8759.
(20) Sun, Z. N.; Wang, H. L.; Liu, F. Q.; Chen, Y.; Tam, P. K. H.; Yang, D. *Org. Lett.* **2009**, *11*, 1887−1890.
(21) Peng, T.; Yang, D. *Org. Lett.* **2010**, *12*, 4932−4935.
(22) Chang, M. C. Y.; Pralle, A.; Isacoff, E. Y.; Chang, C. J. *J. Am. Chem. Soc.* **2004**, *126*, 15392−15393.
(23) Lippert, A. R.; Van de Bittner, G. C.; Chang, C. J. *Acc. Chem. Res.* **2011**, *44*, 793−804.
(24) Zielonka, J.; Sikora, A.; Joseph, J.; Kalyanaraman, B. *J. Biol. Chem.* **2010**, *285*, 14210−14216.
(25) Peng, T.; Wong, N. K.; Chen, X.; Chan, Y. K.; Ho, D. H.; Sun, Z.; Hu, J. J.; Shen, J.; El-Nezami, H.; Yang, D. *J. Am. Chem. Soc.* **2014**, *136*, 11728−11734.
(26) Oushiki, D.; Kojima, H.; Terai, T.; Arita, M.; Hanaoka, K.; Urano, Y.; Nagano, T. *J. Am. Chem. Soc.* **2010**, *132*, 2795−2801.
(27) Jia, X.; Chen, Q.; Yang, Y.; Tang, Y.; Wang, R.; Xu, Y.; Zhu, W.; Qian, X. *J. Am. Chem. Soc.* **2016**, *138*, 10778−10781.
(28) Shuhendler, A. J.; Pu, K.; Cui, L.; Uetrecht, J. P.; Rao, J. *Nat. Biotechnol.* **2014**, *32*, 373−380.
(29) Zhou, X.; Kwon, Y.; Kim, G.; Ryu, J.-H.; Yoon, J. Y. *Biosens. Bioelectron.* **2015**, *64*, 285−291.
(30) Xu, K.; Chen, H.; Tian, J.; Ding, B.; Xie, Y.; Qiang, M.; Tang, B. *Chem. Commun.* **2011**, *47*, 9468−9470.
(31) Tian, J.; Chen, H.; Zhuo, L.; Xie, Y.; Li, N.; Tang, B. *Chem. - Eur. J.* **2011**, *17*, 6626−6634.
(32) Wang, B. S.; Yu, F. B.; Li, P.; Sun, X. F.; Han, K. L. *Dyes Pigm.* **2013**, *96*, 383−390.
(33) Zhou, M.; Diwu, Z.; Panchuk-Voloshina, N.; Haugland, R. P. *Anal. Biochem.* **1997**, *253*, 162−168.
(34) Setsukinai, K. I.; Urano, Y.; Kikuchi, K.; Higuchi, T.; Nagano, T. *J. Chem. Soc., Perkin Trans.* **2000**, *2*, 2453−2457.
(35) Wardman, P. *Free Radical Biol. Med.* **2007**, *43*, 995−1022.
(36) Shepherd, J.; Hilderbrand, S. A.; Waterman, P.; Heinecke, J. W.; Weissleder, R.; Libby, P. *Chem. Biol.* **2007**, *14*, 1221−1231.
(37) Panizzi, P.; Nahrendorf, M.; Wildgruber, M.; Waterman, P.; Figueiredo, J. L.; Aikawa, E.; McCarthy, J.; Weissleder, R.; Hilderbrand, S. A. *J. Am. Chem. Soc.* **2009**, *131*, 15739−15744.
(38) Zhang, Q.; Zhu, Z.; Zheng, Y.; Cheng, J.; Zhang, N.; Long, Y. T.; Zheng, J.; Qian, X.; Yang, Y. *J. Am. Chem. Soc.* **2012**, *134*, 18479−18482.
(39) Setsukinai, K.; Urano, Y.; Kakinuma, K.; Majima, H. J.; Nagano, T. *J. Biol. Chem.* **2003**, *278*, 3170−3175.
(40) Koide, Y.; Urano, Y.; Kenmoku, S.; Kojima, H.; Nagano, T. *J. Am. Chem. Soc.* **2007**, *129*, 10324−10325.
(41) Kalyanaraman, B.; Hardy, M.; Zielonka, J. *Curr. Pharmacol. Rep.* **2016**, *2*, 193−201.
(42) Xu, Q. L.; Lee, K. A.; Lee, S. Y.; Lee, K. M.; Lee, W. J.; Yoon, J. Y. *J. Am. Chem. Soc.* **2013**, *135*, 9944−9949.
(43) Kawagoe, R.; Takashima, I.; Uchinomiya, S.; Ojida, A. *Chem. Sci.* **2017**, DOI: 10.1039/C6SC03856E.
(44) Hou, J. T.; Li, K.; Yang, J.; Yu, K. K.; Liao, Y. X.; Ran, Y. Z.; Liu, Y. H.; Zhou, X. D.; Yu, X. Q. *Chem. Commun.* **2015**, *51*, 6781−6784.
(45) Xu, Z. C.; Baek, K. H.; Kim, H. N.; Cui, J. N.; Qian, X. H.; Spring, D. R.; Shin, I.; Yoon, J. Y. *J. Am. Chem. Soc.* **2010**, *132*, 601−610.
(46) Liu, Z. M.; Feng, L.; Hou, J.; Lv, X.; Ning, J.; Ge, G.-B.; Wang, K. W.; Cui, J. N.; Yang, L. *Sens. Actuators, B* **2014**, *205*, 151−157.
(47) Lim, C. S.; Masanta, G.; Kim, H. J.; Han, J. H.; Kim, H. M.; Cho, B. R. *J. Am. Chem. Soc.* **2011**, *133*, 11132−11135.
(48) Dai, Z. R.; Ge, G. B.; Feng, L.; Ning, J.; Hu, L. H.; Jin, Q.; Wang, D. D.; Lv, X.; Dou, T. Y.; Cui, J. N.; Yang, L. *J. Am. Chem. Soc.* **2015**, *137*, 14488−14495.
(49) Hou, J. T.; Yang, J.; Li, K.; Liao, Y. X.; Yu, K. K.; Xie, Y. M.; Yu, X. Q. *Chem. Commun.* **2014**, *50*, 9947−9950.
(50) Chen, Z. J.; Ren, W.; Wright, Q. E.; Ai, H. W. *J. Am. Chem. Soc.* **2013**, *135*, 14940−14943.
(51) Song, Z. G.; Mao, D.; Sung, S. H. P.; Kwok, R. T. K.; Lam, J. W. Y.; Kong, D. l.; Ding, D.; Tang, B. Z. *Adv. Mater.* **2016**, *28*, 7249−7256.
(52) Liu, F.; Wu, T.; Cao, J.; Zhang, H.; Hu, M.; Sun, S.; Song, F.; Fan, J.; Wang, J.; Peng, X. *Analyst* **2013**, *138*, 775−778.
(53) Chen, Y.; Zhu, C.; Yang, Z.; Chen, J.; He, Y.; Jiao, Y.; He, W.; Qiu, L.; Cen, J.; Guo, Z. *Angew. Chem., Int. Ed.* **2013**, *52*, 1688−1691.
(54) Xu, W.; Teoh, C. L.; Peng, J.; Su, D.; Yuan, L.; Chang, Y. T. *Biomaterials* **2015**, *56*, 1−9.
(55) Sun, Y. Q.; Liu, J.; Zhang, J.; Yang, T.; Guo, W. *Chem. Commun.* **2013**, *49*, 2637−2639.
(56) Yuan, L.; Lin, W. Y.; Yang, Y. T.; Song, J. Z.; Wang, J. L. *Org. Lett.* **2011**, *13*, 3730−3733.
(57) Sun, Q.; Li, J.; Liu, W. N.; Dong, Q. J.; Yang, W. C.; Yang, G. F. *Anal. Chem.* **2013**, *85*, 11304−11311.
(58) Chen, W.; Pacheco, A.; Takano, Y.; Day, J. J.; Hanaoka, K.; Xian, M. *Angew. Chem., Int. Ed.* **2016**, *55*, 9993−9996.
(59) Lee, M. H.; Park, N.; Yi, C.; Han, J. H.; Hong, J. H.; Kim, K. P.; Kang, D. H.; Sessler, J. L.; Kang, C.; Kim, J. S. *J. Am. Chem. Soc.* **2014**, *136*, 14136−14142.
(60) Jiang, N.; Fan, J. L.; Zhang, S.; Wu, T.; Wang, J. Y.; Gao, P.; Qu, J. L.; Zhou, F.; Peng, X. J. *Sens. Actuators, B* **2014**, *190*, 685−693.
(61) Szabo, C.; Ischiropoulos, H.; Radi, R. *Nat. Rev. Drug Discovery* **2007**, *6*, 662−680.
(62) Alvarez, M. N.; Piacenza, L.; Irigoin, F.; Peluffo, G.; Radi, R. *Arch. Biochem. Biophys.* **2004**, *432*, 222−232.
(63) Knight, T. R.; Kurtz, A.; Bajt, M. L.; Hinson, J. A.; Jaeschke, H. *Toxicol. Sci.* **2001**, *62*, 212−220.
(64) Muijsers, R. B. R.; Van den Worm, E.; Folkerts, G.; Beukelman, C. J.; Koster, A. S.; Postma, D. S.; Nijkamp, P. F. *Br. J. Pharmacol.* **2000**, *130*, 932−936.

DOI: 10.1021/jacs.6b10508
J. Am. Chem. Soc. 2017, 139, 285−292

(65) Yuan, L.; Wang, L.; Agrawalla, B. K.; Park, S. J.; Zhu, H.; Sivaraman, B.; Peng, J. J.; Xu, Q. H.; Chang, Y. T. *J. Am. Chem. Soc.* **2015**, *137*, 5930−5938.
(66) Xu, W.; Zeng, Z. B.; Jiang, J. H.; Chang, Y. T.; Yuan, L. *Angew. Chem., Int. Ed.* **2016**, *55*, 13658−13699.
(67) Sun, X. L.; Xu, Q. L.; Kim, G.; Flower, S. E.; Lowe, J. P.; Yoon, J. Y.; Fossey, J. S.; Qian, X. H.; Bull, S. D.; James, T. D. *Chem. Sci.* **2014**, *5*, 3368−3373.

DOI: 10.1021/jacs.6b10508
J. Am. Chem. Soc. 2017, 139, 285−292